Open Access

Communication

Precis. Nanomed. 2025, 8(3):1570-1586

# Therapeutic efficacy of quercetin versus its encapsulated nanoparticle on a tongue squamous cell carcinoma cell line

Hana'a Hezam Algadi*[1,2], Ahmed A. Abd-Rabou[3], Omnia A. Badawi[1], Nada Noureldin[1], Nermine Raouf Amin[1].

[1]*Department of Oral and Maxillofacial Pathology, Faculty of Dentistry, Cairo University, Cairo, Egypt.*

[2]*Department of Oral and Maxillofacial Pathology, Faculty of Dentistry, Hodeidah University, Hodeidah, Yemen*

[3]*Hormones Department, Medical Research and Clinical Studies Institute, National Research Centre, Cairo, Egypt*

Submitted: June 27, 2025 Accepted: August 5, 2025 Published: August 15, 2025

## Graphical Abstract

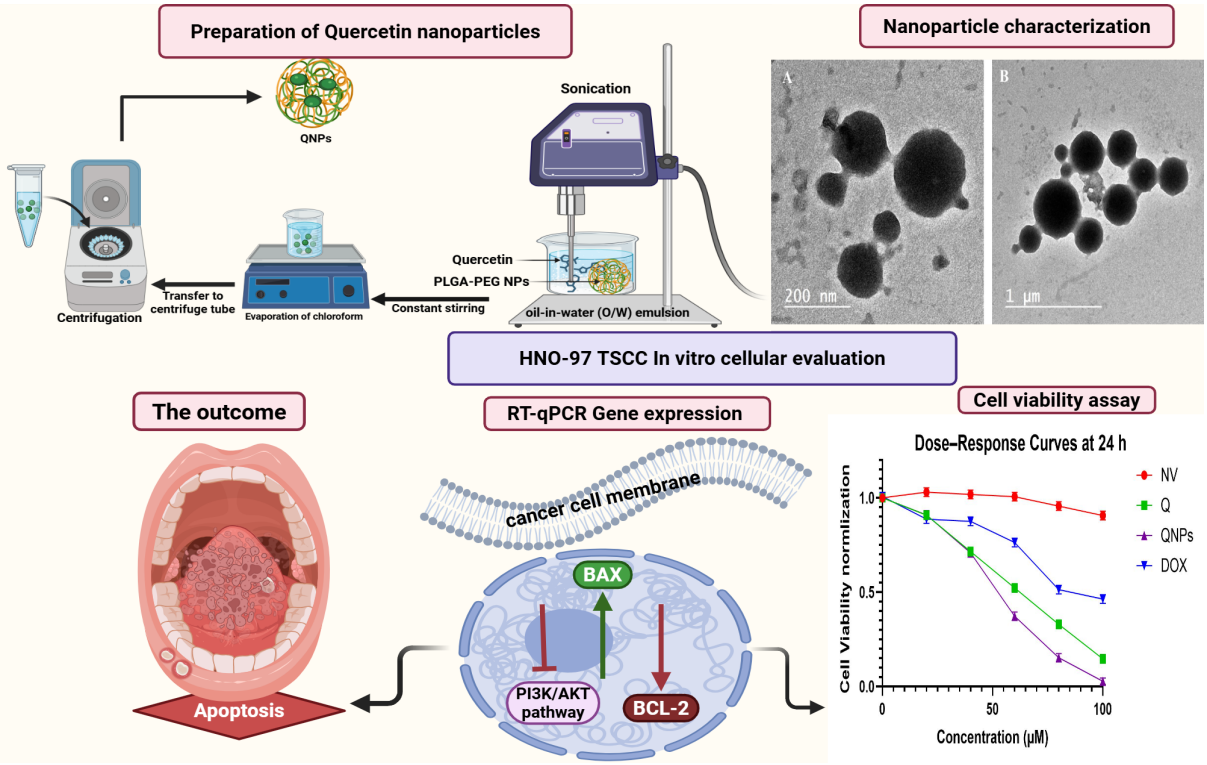


## Abstract

Quercetin, a bioactive flavonoid, has well-documented antitumour properties; however, its clinical application is limited by its hydrophobicity, poor bioavailability, and stability. These limitations can be addressed via the use of nanotechnology-based drug delivery systems. In this study, we aimed to develop polylactide-coglycolide nanoparticles functionalized with polyethylene glycol as a drug vehicle for encapsulating quercetin (QNPs), and further investigate their anticancer potential against the human tongue squamous cell carcinoma cell line HNO-97 by comparing their efficacy with that of free quercetin and doxorubicin, a standard chemotherapeutic control. QNPs were synthesized and characterized

* Corresponding Authors: Hana'a Hezam Algadi, hanaa.ghaleb@dentistry.cu.edu.eg,; Ahmed A. Abd-Rabou, ahmedchemia87@yahoo.com. These authors equally contributed to this work.

for particle size, zeta potential, and entrapment efficiency via dynamic light scattering and for morphology via transmission electron microscopy. Cytotoxicity was evaluated at two time intervals (4 and 24 hours) using the MTT assay. Apoptosis analysis was performed via flow cytometry, and the gene expression levels of Bax, Bcl-2, and PI3K were evaluated via *RT-qPCR*. After 24 hours of treatment, the in vitro cell cytotoxicity study revealed that, compared with free quercetin (59.7 μM) and DOX (74.7 μM), QNPs exhibited superior cytotoxicity ($IC_{50}$ = 41.4 μM). The anticancer efficacy of the QNPs was further confirmed by enhanced cellular apoptosis. Moreover, treating cells with QNPs resulted in an increase in Bax expression levels and a decrease in Bcl-2 and PI3K expression levels, leading to the highest Bax/Bcl-2 ratio. In conclusion, the overall study results suggest that quercetin encapsulated PLGA-PEG nanoparticles may serve as potential drug candidates for the treatment of human tongue squamous cell carcinoma.

Keywords: Tongue cancer cell line; HNO-97 cell line; anticancer; phytochemicals; quercetin; PLGA-PEG nanoparticles; PI3K/AKT pathway; BAX/BCL-2 ratio.

## Rationale, Purpose, and Limitations

Human tongue squamous cell carcinoma (TSCC) is a highly aggressive malignancy with limited therapeutic options and significant treatment-related morbidity. Although quercetin (Q) demonstrates notable anticancer activity, its clinical application is restricted by poor aqueous solubility, low bioavailability, and limited stability. This study addresses these challenges by encapsulating Q within PLGA-PEG nanoparticles (QNPs) and assessing their anticancer efficacy in the HNO-97 TSCC cell line, compared to free Q and doxorubicin (DOX). The results indicate that QNPs significantly improve cellular uptake, cytotoxicity, and proapoptotic gene modulation, suggesting their potential as a targeted nanotherapeutic strategy for TSCC. Nonetheless, the study's in vitro design does not fully mimic the tumor microenvironment or systemic drug behavior. Further in vivo studies and detailed mechanistic investigations, including mitochondrial and caspase pathway analyses, are required to substantiate these findings and support clinical translation.

## Introduction

TSCC is the most aggressive subtype of oral squamous cell carcinoma (OSCC) and is characterized by high locoregional recurrence and a poor prognosis. Traditional treatment for TSCC includes surgery with or without adjuvant chemoradiotherapy. Although these modalities have contributed significantly to the treatment of TSCC, they are associated with comorbidities and reduced quality of life, which underscores the urgent need for alternative natural therapeutic modalities [1-3].

The application of natural phytochemicals is considered an efficient and safer alternative therapeutic strategy. They have gained increasing attention as emerging areas in anticancer research [4]. Among dietary polyphenolic compounds, quercetin (Q), a bioactive flavonoid with strong antioxidant and anti-inflammatory properties, is found in various fruits (e.g., apples, blueberries, watermelon) and vegetables (e.g., corn, onions, tofu) and is also present in beverages such as tea and wine [5]. It has shown notable anticancer effects in various malignancies[6-10]. Q interferes with several cellular processes involved in cancer development, mainly through the inhibition of proliferation [9], suppression of metastasis [11], triggering of apoptosis [12], and blocking of cancer-associated angiogenesis [13].

Owing to their poor solubility in water and short half-life (approximately 11–24 hours), NP-based drug delivery systems are considered innovative strategies to improve their efficacy by releasing a bioactive drug at a specific site that targets malignant cells, increasing its solubility and dissolution, increasing its bioavailability and biodistribution, increasing its stability, and controlling and extending its duration of release at the primary location of malignant tumors [14, 15].

Among various nanocarriers, polymeric NPs have distinct merits, such as small particle sizes, which promote tissue penetration and targeting refinement. In addition to synthesis simplicity, extended clearance time from the body, decreased toxicity, biocompatibility, and biodegradability are desirable. Synthetic polymers such as polylactic-co-glycolic acid (PLGA), poly ε-caprolactone (PCL), and polylactic acid (PLA) are more widely studied since their chemical and physical properties are favourable [16, 17].

The amphiphilic copolymer PLGA–polyethylene glycol (PLGA-PEG) is especially attractive as a nanocarrier system. This aligns in such a manner that hydrophobic oily PLGA stills inside, increasing the stability and bioavailability

of the therapeutic drug. The hydrophilic PEG shell is outside the polymer, acting as a stabilizing frame, controlling the release of the therapeutic agent from the core and preventing the recognition of the NPs by immune cells [17, 18]. Several in vitro and in vivo studies have demonstrated that Q induces cytotoxicity and apoptosis in OSCC [19-22]; however, few investigations have explored its efficacy in treating TSCC [23]. To the best of our knowledge, no study has yet examined the anticancer potential of Q encapsulated in PLGA-PEG NPs (QNPs) against the HNO-97 TSCC cell line.

The present study investigated the potential of QNPs for treating TSCC. This study aimed to evaluate the therapeutic efficacy of QNPs in the HNO-97 TSCC cell line compared with that of free Q, with doxorubicin (DOX) serving as the standard chemotherapeutic control. The evaluation included the assessment of cytotoxicity, apoptosis investigation, flow cytometric analysis, and the expression levels of the proapoptotic (Bax) and antiapoptotic (Bcl-2) genes, as well as the PI3K gene.

## Materials and methods

### Chemicals and reagents

Quercetin (Q; ≥95%, HPLC grade), poly($_{D,L}$-lactide-co-glycolide) (PLGA, copolymer ratio 50:50), polyethylene glycol (2 kDa), doxorubicin hydrochloride (2 mg/mL), and polyvinyl alcohol (PVA, MW 30.000) were used. MTT reagent [3-(4,5-dimethylthiazol-2-yl)-2,5-diphenyltetrazolium bromide] and chloroform were purchased from Sigma–Aldrich (St. Louis, MO, USA). Fetal bovine serum (FBS) and 1× trypsin-EDTA solution (0.25% trypsin, 0.02% EDTA) were purchased from Biowest (USA). Phosphate-buffered saline (PBS) was obtained from SEROX (Germany). The Annexin V-FITC/Propidium Iodide (PI) Kit, RevertAid First-Strand cDNA Synthesis Kit, and RNA Purification Kit were purchased from Thermo Fisher Scientific (USA). The MiScript SYBR Green PCR Kit was procured from Qiagen (Valencia, CA, USA). Ultrapure water (Milli-Q) was used throughout all the experiments (Millipore, Bedford, MA, USA).

### Preparation of PLGA-PEG Nanoparticles and QNPs

A modified oil-in-water (O/W) single-emulsion solvent evaporation method was used to synthesize the PLGA-PEG NPs. The organic phase was prepared by dissolving 100 mg of PLGA in 3 mL of chloroform. Separately, the aqueous phase was prepared by dissolving 5 mg of PEG (MW = 2 kDa) and 2% (w/v) PVA in 12 mL of double-distilled water [24]. The organic phase was slowly added dropwise to the aqueous PEG/PVA solution under continuous stirring, followed by emulsification via a microtip probe sonicator (VC 505, VibraCell™, Sonics & Materials, Newton, USA) operated at 55 W for 2 minutes in an ice bath (Thermo Scientific™, USA) to maintain thermal stability. This process generated a stable O/W emulsion. The emulsion was then stirred overnight at room temperature via a magnetic stirrer (VELP Scientifica Srl, Italy) to allow complete chloroform evaporation. NPs were harvested by ultracentrifugation at 50,602 ×g for 20 minutes at 4°C (OHAUS, Germany), and the pellet was washed three times with double-distilled water to eliminate unencapsulated components and residual surfactant. For the preparation of the QNPs, Q was codissolved with PLGA in the organic phase before emulsification. Various formulations were prepared to evaluate drug-loading capacity and encapsulation efficiency.

### Nanoparticle characterization

#### *Assessment of particle size, zeta potential, and polydispersity index*

The particle size, zeta potential, and polydispersity index (PDI) of PLGA-PEG nanovoids (NVs) (i.e., nanoparticles without loaded Q) and QNPs were determined via dynamic light scattering (DLS) with a Zetasizer (Nano ZS, Malvern Instruments Ltd., UK). All measurements were performed in triplicate at a constant temperature of 25.0 °C to ensure reproducibility and accuracy.

#### *Measurement of the Entrapment Efficiency and Drug-Loading Content*

The entrapment efficiency (EE) and drug-loading content (DLC) are critical parameters for quantifying the percentage of Q successfully incorporated into PLGA-PEG NPs. The EE (%) and DLC (%) of QNPs were quantitatively assessed using a validated UV–Vis spectrophotometric method at 370 nm following centrifugation and separation of unencapsulated quercetin. The EE% and DLC% were calculated using the following equations:

Entrapment Efficiency (EE%) = (Weight of encapsulated drug / Initial drug weight) × 100.

Drug-Loading Content (DLC%) = (Weight of encapsulated drug / Total weight of nanoparticles) × 100.

### *Transmission electron microscopy*

The particle morphology of the NVs and QNPs was assessed via transmission electron microscopy (TEM; JEOL JEM-2100, Japan). In brief, 50 µL of the QNPs solution was dropped onto Formvar-coated copper grids, after which the samples were stained with 2% (w/v) uranyl acetate. Digital micrographs and soft imaging viewer software were used for image capture and analysis (Electron Microscope Unit Services), National Research Centre, Egypt.

### *Cellular Uptake Assay*

Q and QNPs were labeled with Alexa Fluor 488 NHS ester (Thermo Fisher Scientific) to enable fluorescence-based detection. Briefly, Q or QNPs were suspended in 0.1 M sodium bicarbonate buffer (pH=8.3) and incubated with Alexa Fluor 488 NHS ester at a molar ratio of 1:10 (Q: dye) for 1 hour at room temperature in the dark. Unreacted dye was removed by dialysis against PBS (pH=7.4) using a 3.5 kDa molecular weight cut-off (MWCO) dialysis membrane for 24 hours at 4°C, with buffer changes every 4 hours. Cells were treated with Alexa Fluor 488-labeled Q or QNPs at concentrations corresponding to their respective $IC_{50}$ values (determined by prior cytotoxicity assays) for 0, 4, and 24 hours. After each time point, cells were washed with PBS, trypsinized, and resuspended in cold PBS for analysis. Cellular uptake was quantified using flow cytometry (BD FACS) by measuring the mean fluorescence intensity (MFI) of Alexa Fluor 488 within the cells. A minimum of 10,000 events was recorded per sample. Data were analyzed using FlowJo software. Fluorescence intensities were normalized and expressed as relative percentage uptake.

## In vitro studies

### *Cell culture*

The human TSCC cell line HNO-97 (# RRID: CVCL_D227) was purchased from the American Type Culture Collection through Nawah-Scientific, Almokattam, Cairo, Egypt. The HNO-97 cell line used in this study was authenticated via short tandem repeat (STR) profiling, which confirmed its identity by matching its STR profile to publicly available reference databases (Cellosaurus). No cross-contamination or misidentification was detected. The cells were cultivated with Dulbecco's modified Eagle's medium (DMEM). All media were supplied with 1% L-glutamine, 1% PBS, and 10% FBS. The cells were incubated in 5% $CO_2$ in a humidified incubator at 37°C (Binder, Germany) for maintenance of cellular expansion.

### *Cell viability assay*

HNO-97 cells were cultured in 96-well plates at a density of $5 \times 10^3$ cells/well and incubated for one day. Following incubation, the cultured cells were treated with various concentrations (20, 40, 60, 80, and 100 µM) of Q, QNPs, DOX, and NVs for 4 and 24 hours. Additionally, the control cells were maintained without any treatment. After adding 5 mg/ml of the dissolved MTT in PBS to each well, the tested agents were incubated for 4 hours at 37°C. Water-insoluble dark blue formazan crystals that resulted from MTT cleavage in actively metabolized cells were then dissolved in DMSO. The absorbance of the resulting color solution was measured at A455 nm via an ELISA microplate reader (Model 500; BIO RAD Instrument Inc., USA). The cell viability (%) was calculated via the following equation [25]:

Cell viability (%) = (mean absorbance of treated cells/mean absorbance of control cells) × 100.

### *Measurement of the half-inhibitory concentration*

The half-maximal inhibitory concentration ($IC_{50}$) represents the concentration of the experimental agent required to reduce the viability of HNO-97 TSCC cells by 50%. To determine the $IC_{50}$ values, the percentages of viable cells were plotted against sample concentrations using polynomial concentration-response curve fitting models (OriginPro 8 software).

### *Flow cytometry-based apoptosis assay*

HNO-97 cells were seeded at a density of $1 \times 10^6$ cells/T25 flask and incubated for 24 hours. The cells were treated with the $IC_{50}$ values of the NVs, Q, QNPs, and DOX and incubated for 4 and 24 hours. After one day, annexin V-FITC and PI staining were performed on all the samples. The apoptotic distributions of the treated and untreated cells were evaluated via flow cytometry (Beckman Coulter Instrument, USA). A total of 25000 events were registered

per sample and analyzed via FlowJo-V10 software.

### *Quantitative real-time RT-qPCR*

To investigate the molecular mechanisms underlying apoptosis, HNO-97 cells were treated with the optimal $IC_{50}$ of all the experimental formulations, which is the most effective anticancer concentration based on the MTTA results. Total RNA was subsequently extracted from HNO-97 cells via the Invitrogen RNA Purification Kit following the manufacturer's protocol. The concentration and purity of the RNA were determined via a NanoDrop UV spectrophotometer (Thermo Fisher Scientific, USA). The Revert Aid First-Strand cDNA Synthesis Kit was used to generate complementary DNA (cDNA) from 1 µg of total RNA following the manufacturer's instructions. These samples were subsequently frozen at a temperature of –80°C until they were used for determination of the expression levels of the Bax, Bcl-2, and PIK3 genes via the quantitative real-time polymerase chain reaction (PCR) (*RT-qPCR)* which were subsequently performed via the DT-lite Real-Time PCR System (English/Russian system, DNA-Technology, Russia, Moscow) with the required components (including the SYBR Green PCR, the forward and reverse primers for each gene, and a buffer solution). Gene expression levels of the Bax, Bcl-2, and PI3K genes were evaluated. GAPDH was utilized as the internal control (housekeeping) gene. The primer sequences are provided in Table 1. A total of 10 µL of SYBR Green Master Mix, 1 µL of each primer (400 nM), 1 µL of cDNA, and 7 µL of RNase-free water made up the entire 20 µL PCR mixture. Initial activation was performed at 95°C for 15 minutes, after which 40 cycles of denaturation at 95°C for 30 seconds, annealing at 55°C for 30 seconds, and extension at 72°C for 30 seconds were performed. After RT–PCR, the products were analyzed via melt–curve analysis with the default settings to clarify the exact amplification of the intended single products. The primer efficiency was verified via standard curve analysis. The relative expression levels of the target genes were calculated via the $2^{-\Delta\Delta Cq}$ method [26], and all the fold-change values were log-transformed before statistical analysis. Gene expression was quantified from triplicate reactions for each condition.

Table 1. Primer sequences

| Primer | Sequence from 5′- 3′ |
|---|---|
| BCL2 | Forward 5'-CTGCACCTGACGCCCTTCACC-3' |
| | Reverse 5'-CACATGACCCCACCGAACTCAAAGA-3' |
| Bax | Forward 5'-ATGGCTTCTATGAGGCTGAG-3' |
| | Reverse 5'-CGGCCCCAGTTGAAGTTG-3' |
| PI3K | Forward 5'-GCTCTCGGTTGATTCCAACGT-3' |
| | Reverse 5'-ATGGCTTCTATGAGGCTGAG-3' |
| GAPDH | Forward 5'-GTCTCCTCTGACTTCAACAGCG-3' |
| | Reverse 5'-ACCACCCTGTTGCTGTAGCCAA-3' |

### Statistical analysis

All experiments were repeated three times (n = 3), and each experimental condition was tested in technical triplicate. Numerical data were explored for normality by checking the distribution of the data and using tests of normality (Kolmogorov–Smirnov and Shapiro–Wilk tests). All the data had a normal (parametric) distribution. The data are presented as the means and standard deviations (SDs). Repeated-measures ANOVA was used to compare data between and within the groups. Bonferroni post hoc correction was used for pairwise comparisons when the ANOVA test was significant. The significance level was set at $P \leq 0.05$. Statistical analysis was performed with IBM SPSS Statistics for Windows, version 23.0. Armonk, NY: IBM Corp.

## Results

### Nanoparticle characterization

#### *Transmission Electron Microscopy*

Figure 1A shows spherical-shaped particles, with particle sizes ranging from 73 to 155 nm. As shown in Figure 1B, the configuration of the QNPs that appeared in the TEM image exhibited a distinct core–shell structure, in which Q was encapsulated within the core and surrounded by a PLGA–PEG shell. The average size of the QNPs ranged from 150 to 290 nm.

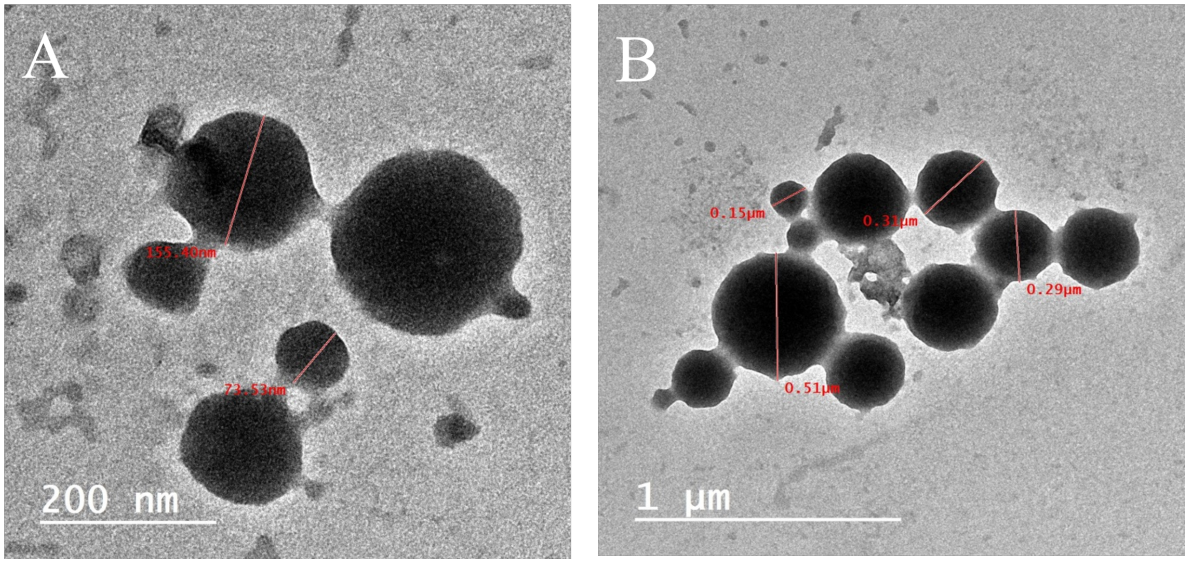


*Figure 1. TEM images illustrating the shape and size of measured nanoparticles: (A) morphology and size of PLGA-PEG nanovoids (NVs); (B) morphology and size of QNPs*

#### *Assessment of Particle Size, Zeta Potential, and Polydispersity Index*

DLS analysis revealed Z-average diameters of the NVs and QNPs of 141.80+2.01 nm and 220.20+1.50 nm, respectively. The observed increase in particle size following Q loading suggested successful encapsulation of Q within the PLGA-PEG matrix. The PDI values were very low at 0.07+0.00 for the NVs and 0.02+0.00 for the QNPs, indicating uniform dispersion. The zeta potential values of -28.90+0.57 mV for the NVs and -32.50+1.03 mV for the QNPs reflected a sufficient surface charge to maintain colloidal stability and reduced particle aggregation.

#### *Entrapment Efficiency (EE) and Drug-Loading Content (DLC):*

The high EE of the QNPs was 85.4 ±1.02%, demonstrating high drug-loading capacity and effective incorporation of Q into the PLGA-PEG NPs. Furthermore, the drug-loading content was determined to be 12.7 ± 0.86%, indicating substantial Q incorporation relative to the total NPs mass. These findings reflected the strong affinity of Q for the hydrophobic PLGA core and the successful formulation strategy adopted.

#### *Cellular Uptake of Alexa Fluor 488-Labeled Q and QNPs*

The cellular uptake of Alexa Fluor 488–labeled Q and QNPs in HNO-97 cells was evaluated by flow cytometry at 0-, 4-, and 24-hours using $IC_{50}$ concentrations. As shown in Figure 2, at 0 hours, both groups showed negligible fluorescence (<0.5%), confirming no immediate uptake or surface binding.

At 4 hours, Q exhibited higher uptake (38.5%) compared to QNPs (31.3%), suggesting faster internalization of free Q due to its smaller size and passive diffusion. However, by 24 hours, QNPs-treated cells showed significantly greater uptake (92.2%) versus Q (55.3%), indicating enhanced time-dependent internalization via NPs-mediated delivery. These results demonstrate that QNPs enable sustained and higher intracellular accumulation over time, while free Q shows faster but limited uptake. The uptake profile supports a sustained release mechanism and efficient endocytic uptake of QNPs.

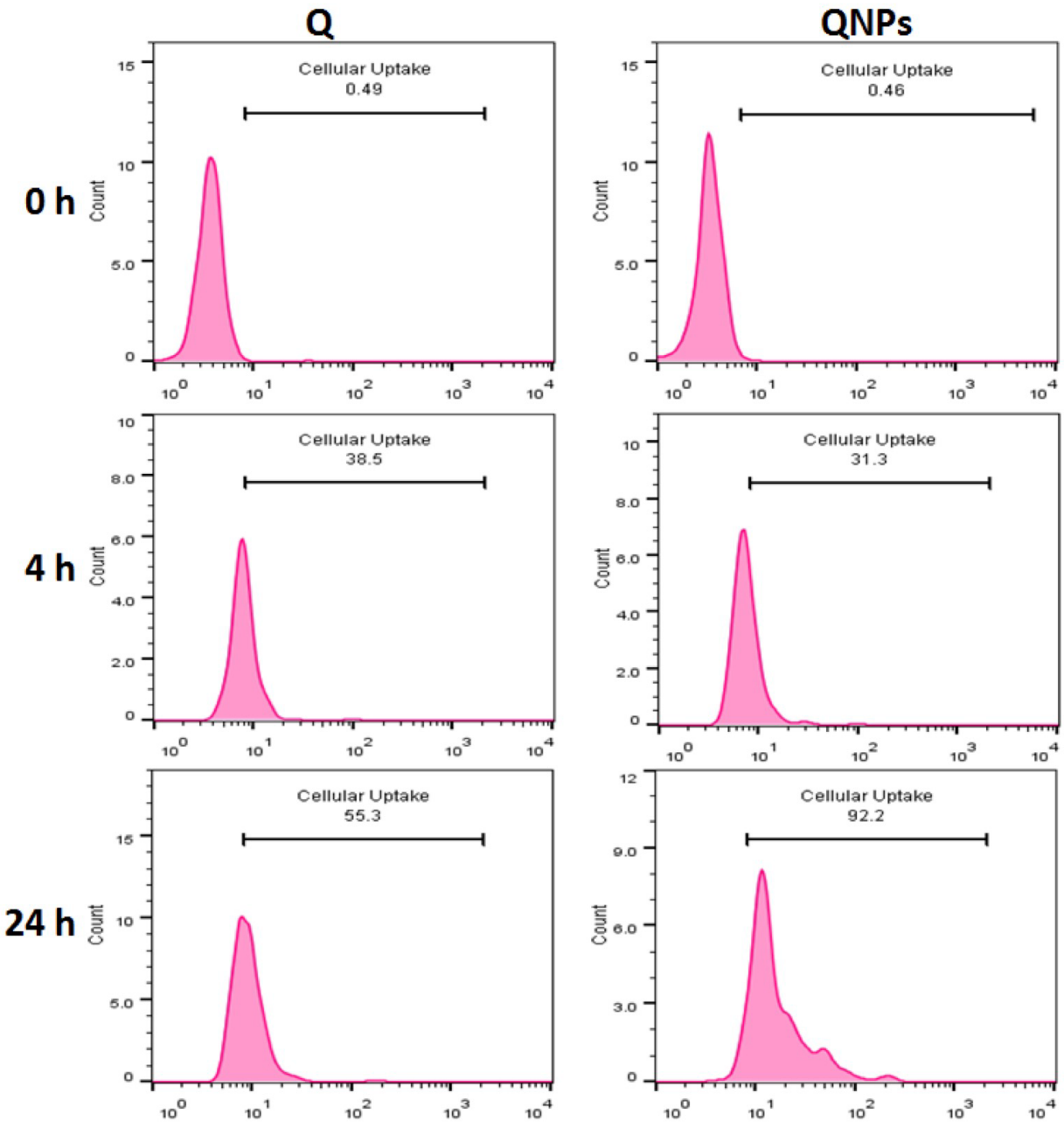


*Figure 2. Flow cytometry analyses of the cellular uptake of Q and QNPs in HNO-97 cells after 0-, 4-, and 24-hour incubation using $IC_{50}$ concentrations.*

## In vitro studies

### *Cytotoxicity*

The antiproliferative effects of Q, the QNPs, the NVs, and the positive control DOX on HNO-97 cells were evaluated via the MTT assay at concentrations of 20, 40, 60, 80, and 100 µM following 4 and 24 hours of incubation. As shown in Table 2, cell viability significantly decreased in a dose- and time-dependent manner for all the active treatments. Compared with free Q and DOX, the QNPs showed superior cytotoxicity at higher concentrations and more extended incubation periods.

After 4 hours, cell viability was reduced to 44.90% with 100 µM QNPs, whereas it was 18.30% with Q and 32.20% with DOX. After 24 hours, the QNPs had a more pronounced cytotoxic effect, reducing the viability to 2.60% at the same concentration, versus 14.00% for Q and 44.40% for DOX. NVs-treated cells maintained high viability across all concentrations

and time intervals (>87%), confirming the biocompatibility of the PLGA-PEG matrix. Statistical analysis revealed significant differences between groups at all concentrations and time intervals ($P < 0.001$), with partial eta squared ($\eta^2$) values ranging from 0.343 to 0.996.

Table 2. Cell viability (%) of HNO-97 TSCC cells following treatment with various concentrations of Q, QNPs, NVs, and DOX after 4 and 24 hours.

| Time | Conc. (µM) | NVs | | Q | | QNPs | | DOX | | *P* value | $\eta^2$ |
|---|---|---|---|---|---|---|---|---|---|---|---|
| | | Mean | SD | Mean | SD | Mean | SD | Mean | SD | | |
| 4 hours | 20 | 95.70 $^{A}$ | 2.4 | 87.60 $^{C}$ | 2.30 | 89.60 $^{B}$ | 0.30 | 90.30 $^{B}$ | 2.30 | <0.001* | 0.343 |
| | 40 | 93.40 $^{A}$ | 2.30 | 73.80 $^{C}$ | 2.10 | 78.40 $^{B}$ | 2.10 | 76.40 $^{B}$ | 2.10 | <0.001* | 0.772 |
| | 60 | 91.10 $^{A}$ | 2.30 | 48.40 $^{D}$ | 1.90 | 64.50 $^{B}$ | 2.00 | 51.02 $^{C}$ | 1.90 | <0.001* | 0.944 |
| | 80 | 91.10 $^{A}$ | 2.30 | 22.90 $^{D}$ | 1.90 | 50.70 $^{B}$ | 1.90 | 36.80 $^{C}$ | 1.80 | <0.001* | 0.974 |
| | 100 | 88.80 $^{A}$ | 2.30 | 18.30 $^{D}$ | 1.90 | 44.90 $^{B}$ | 1.90 | 32.20 $^{C}$ | 1.90 | <0.001* | 0.976 |
| 24 hours | 20 | 98.80 $^{A}$ | 0.03 | 87.10 $^{B}$ | 0.30 | 87.20 $^{B}$ | 0.30 | 85.10 $^{C}$ | 0.30 | <0.001* | 0.878 |
| | 40 | 97.70 $^{A}$ | 0.05 | 68.60 $^{C}$ | 0.70 | 67.90 $^{C}$ | 0.70 | 84.00 $^{B}$ | 0.40 | <0.001* | 0.974 |
| | 60 | 96.50 $^{A}$ | 0.08 | 50.10 $^{C}$ | 1.10 | 35.70 $^{D}$ | 1.40 | 73.20 $^{B}$ | 0.60 | <0.001* | 0.992 |
| | 80 | 91.70 $^{A}$ | 0.20 | 31.60 $^{C}$ | 1.50 | 14.60 $^{D}$ | 1.90 | 49.20 $^{B}$ | 1.10 | <0.001* | 0.995 |
| | 100 | 86.90 $^{A}$ | 0.30 | 14.00 $^{C}$ | 1.90 | 2.60 $^{D}$ | 1.60 | 44.40 $^{B}$ | 1.20 | <0.001* | 0.996 |

$^{A, B, C, D}$ Different superscripts in the same row indicate statistically significant differences between experimental formulations; DOX, doxorubicin; NVs, PLGA-PEG nanovoids; Q, quercetin; and QNPs, quercetin-loaded PLGA-PEG nanoparticles. *Significant, $P \leq 0.05$; $\eta^2$, Effect size (Partial Eta Squared).

### *$IC_{50}$ analysis*

$IC_{50}$ values, another measure of cytotoxicity, were calculated to quantify the half-maximal inhibitory concentration for HNO-97 cell growth; the more cytotoxic the drug was, the lower the $IC_{50}$ value. After 24 hours, as revealed in Table 3, the QNPs had the lowest $IC_{50}$ value (41.40 ± 1.30 µM), which was significantly lower than that of Q (59.70 ±1.30 µM) and DOX (74.70 ± 1.30 µM) ($P < 0.001$, $\eta^2 = 0.993$). In contrast to Q (58.80 ± 1.20 µM), the QNPs showed superior cytotoxicity after 24 hours, confirming their time-dependent efficacy due to their sustained release, despite having a comparatively higher $IC_{50}$ value at 4 hours (70.50 ± 1.30 µM).

### *Apoptosis-mediated cancer cell death*

Apoptotic cell death in HNO-97 cells was assessed using Annexin V-FITC/PI flow cytometry after treatment with the $IC_{50}$ concentrations of Q, QNPs, DOX, and NVs for 4 and 24 hours. As shown in Table 4, after 4 hours of incubation, Q reduced the viable cell population from 97.22% (control) to 10.05%, while increasing early and late apoptosis rates to 34.63% and 41.64%, respectively. The QNPs exhibited minimal apoptotic induction at this early time point. DOX, used as a positive control for apoptosis, reduced the viable cell population from 97.22% to 33.96%, with early and late apoptosis increasing to 15.57% and 48.93%, respectively, and minimal necrosis (1.19%).

After 24 hours of incubation, the QNPs had the most significant proapoptotic effect, reducing the percentage of viable cells to 0.31% and increasing the percentage of late apoptotic cells to 87.61%, outperforming both the Q (41.69%) and DOX (61.46%) treatments. For further illustration, Figure 3 shows that after 4 hours of incubation, There was a notable shift in the cell populations from the viable quadrant (Annexin $V^-/PI^-$) to the early and late apoptotic quadrants (Annexin $V^+/PI^-$ and Annexin $V^+/PI^+$), especially after 24 hours of incubation.

Table 3. $IC_{50}$ values (μM) of Q, QNPs, and DOX in HNO-97 TSCC cells after 4 and 24 hours of treatment.

| Time | Q | | QNPs | | DOX | | *P* value | $\eta^2$ |
|---|---|---|---|---|---|---|---|---|
| | Mean | SD | Mean | SD | Mean | SD | | |
| 4 hours | 58.80 $^{C}$ | 1.20 | 70.50 $^{A}$ | 1.30 | 63.10 $^{B}$ | 1.30 | <0.001* | 0.946 |
| 24 hours | 59.70 $^{C}$ | 1.30 | 41.40 $^{A}$ | 1.30 | 74.70 $^{B}$ | 1.30 | <0.001* | 0.993 |

$^{A,B,C}$Different superscripts in the same row indicate statistically significant differences between experimental formulations; DOX, doxorubicin; Q, quercetin; and QNPs, quercetin-loaded PLGA-PEG nanoparticles. *Significant, $P \leq 0.05$; $\eta^2$, effect size (partial eta squared).

Table 4. Annexin V-FITC/PI-based flow cytometric analysis of apoptosis in HNO-97 TSCC cells after 4 and 24 hours of treatment with $IC_{50}$ concentrations of Q, NVs, QNPs, and DOX.

| Time | Apoptosis | Control | | NVs | | Q | | QNPs | | DOX | | P value | $\eta^2$ |
|---|---|---|---|---|---|---|---|---|---|---|---|---|---|
| | | Mean | SD | Mean | SD | Mean | SD | Mean | SD | Mean | SD | | |
| 4 h | Unapoptotic | $97.22^{A}$ | 0.14 | $95.36^{B}$ | 0.06 | $10.05^{E}$ | 0.22 | $85.97^{C}$ | 0.09 | $33.96^{D}$ | 0.12 | <0.001* | 0.999 |
| | Early Apoptotic | $2.12^{CD}$ | 0.07 | $2.15^{D}$ | 0.05 | $34.63^{A}$ | 0.10 | $3.71^{C}$ | 0.10 | $15.57^{B}$ | 0.13 | <0.001* | 0.999 |
| | Late Apoptotic | $0.25^{E}$ | 0.30 | $1.02^{D}$ | 0.14 | $41.64^{B}$ | 0.16 | $5.43^{C}$ | 0.28 | $48.93^{A}$ | 0.17 | <0.001* | 0.999 |
| | Necrotic | $0.50^{E}$ | 0.33 | $1.33^{C}$ | 0.16 | $13.31^{A}$ | 0.14 | $4.67^{B}$ | 0.10 | $1.19^{D}$ | 0.21 | <0.001* | 0.998 |
| 24 h | Unapoptotic | $97.83^{A}$ | 0.37 | $92.53^{B}$ | 0.19 | $5.25^{D}$ | 0.12 | $0.31^{E}$ | 0.26 | $17.78^{C}$ | 0.29 | <0.001* | 0.999 |
| | Early Apoptotic | $0.96^{E}$ | 0.34 | $2.22^{D}$ | 0.42 | $50.03^{A}$ | 0.13 | $12.12^{C}$ | 0.31 | $19.10^{B}$ | 0.19 | <0.001* | 0.999 |
| | Late Apoptotic | $0.19^{E}$ | 0.15 | $2.61^{D}$ | 0.17 | $41.69^{C}$ | 0.29 | $87.61^{B}$ | 0.22 | $61.46^{A}$ | 0.13 | <0.001* | 0.999 |
| | Necrotic | $0.67^{C}$ | 0.26 | $2.68^{B}$ | 0.46 | $2.90^{A}$ | 0.01 | $0.30^{D}$ | 0.30 | $2.16^{AB}$ | 0.10 | <0.001* | 0.969 |

$^{A,B,C,D}$ Different superscripts in the same row indicate statistically significant differences between experimental formulations; DOX, doxorubicin; Q, quercetin; and QNPs, quercetin-loaded PLGA-PEG nanoparticles. *Significant, $P \leq 0.05$; $\eta^2$, effect size (partial eta squared).

### *Gene expression of Bax, Bcl-2, and PI3K*

As presented in Table 5, the expression of apoptosis-related genes was significantly affected following QNPs treatment for 4 and 24 hours. At 4 hours, compared with those in the control and NVs groups, the expression of Bax (2.50-fold) was upregulated, and the expression of Bcl-2 (0.18-fold) and PI3K (0.33-fold) ($P < 0.001$) was downregulated. After 24 hours, Bax expression increased 2.77-fold, Bcl-2 expression decreased 0.09-fold, and PI3K expression was reduced 0.08-fold ($P < 0.001$). These results indicated that Q encapsulation in PLGA-PEG increased its ability to modulate apoptotic and survival signalling pathways, surpassing the efficacy of both free Q and DOX

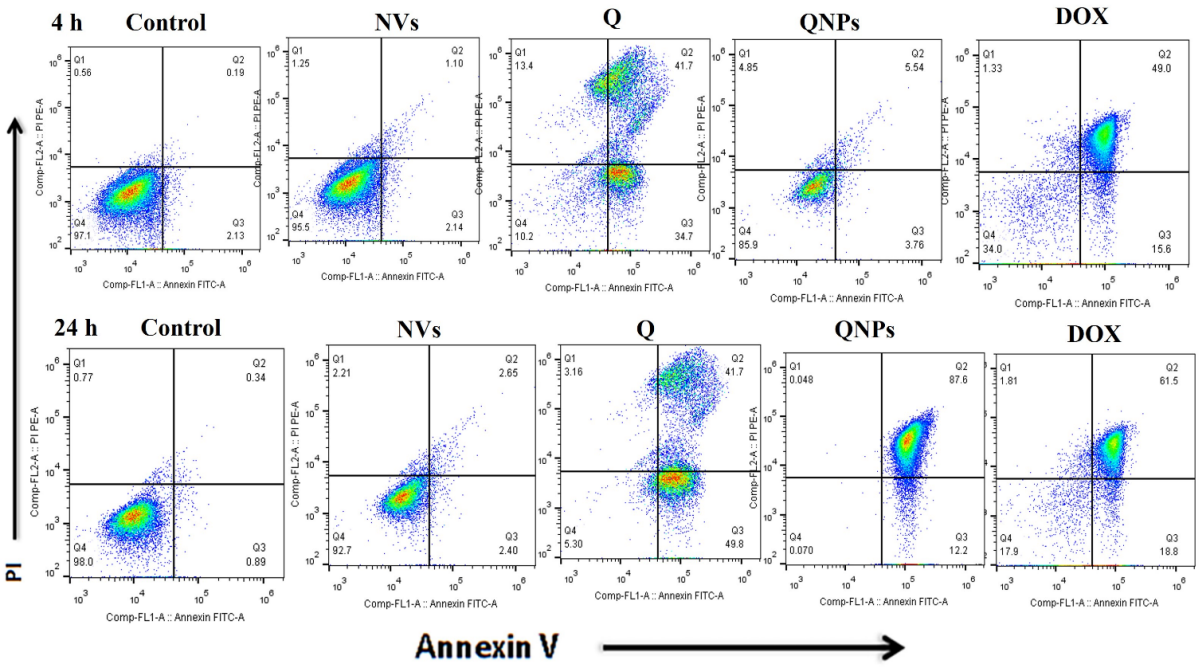


*Figure 3. Histogram for Annexin V-FITC/PI-based flow cytometric analysis of apoptosis in HNO-97 TSCC cells after 4 and 24 hours of treatment with $IC_{50}$ concentrations of Q, NVs, QNPs, and DOX.*

Table 5. Genetic profiling via real-time *qPCR* of Bcl-2, Bax, and PI3K in HNO-97 TSCC cells after treatment with $IC_{50}$ concentrations of Q, QNPs, and DOX compared with those in the control and NVs groups after 4 and 24 hours of incubation.

| Time | gene | NVs | | Q | | QNPs | | DOX | | *P* value | $\eta^2$ |
|---|---|---|---|---|---|---|---|---|---|---|---|
| | | Mean | SD | Mean | SD | Mean | SD | Mean | SD | | |
| 4 h | Bax | 1.05 $^{D}$ | 0.01 | 1.89 $^{B}$ | 0.02 | 2.50 $^{A}$ | 0.01 | 1.63 $^{C}$ | 0.03 | <0.001* | 0.998 |
| | Bcl-2 | 1.01 $^{A}$ | 0.02 | 0.42 $^{C}$ | 0.01 | 0.18 $^{D}$ | 0.01 | 0.67 $^{B}$ | 0.02 | <0.001* | 0.994 |
| | Pl3k | 0.89 $^{A}$ | 0.01 | 0.56 $^{B}$ | 0.01 | 0.33 $^{C}$ | 0.03 | 0.58 $^{B}$ | 0.01 | <0.001* | 0.986 |
| 24 h | Bax | 1.00 $^{D}$ | 0.01 | 2.26 $^{B}$ | 0.02 | 2.77 $^{A}$ | 0.01 | 2.00 $^{C}$ | 0.03 | <0.001* | 0.999 |
| | Bcl-2 | 1.00 $^{A}$ | 0.01 | 0.36 $^{B}$ | 0.01 | 0.09 $^{C}$ | 0.01 | 0.39 $^{B}$ | 0.02 | <0.001* | 0.996 |
| | Pl3k | 0.91 $^{A}$ | 0.02 | 0.32 $^{B}$ | 0.01 | 0.08 $^{C}$ | 0.01 | 0.30 $^{B}$ | 0.01 | <0.001* | 0.995 |

$^{A,B,C,D}$ Different superscripts in the same row indicate statistically significant differences between experimental formulations; DOX, doxorubicin; NVs, PLGA-PEG nanovoids; Q, quercetin; and QNPs, quercetin-loaded PLGA-PEG nanoparticles. *Significant, $P \leq 0.05$; $\eta^2$, Effect size (Partial Eta Squared).

### *3.2.4. Bax/Bcl-2 ratio*

The Bax/Bcl-2 ratio, a critical marker of apoptosis, was calculated by dividing the fold change in the Bax gene by the Bcl-2 gene. A ratio > 1 indicates the proapoptotic activity of the experimental agent, and if the ratio <1, it indicates antiapoptotic activity. As shown in Table 6, the QNPs produced the highest Bax/Bcl-2 ratios of 13.92 at 4 hours and 31.03 at 24 hours. This value was significantly greater than those of Q (4.54 and 6.34) and DOX (2.43 and 5.13) ($P < 0.001$). NVs had no significant effect, maintaining baseline ratios close to 1.

## Discussion

Nanotechnology-based cancer therapies have emerged as promising strategies to improve the therapeutic efficacy of anticancer agents by increasing their bioavailability and targeting efficiency [27-29]. The nano-combination of PLGA-PEG is a promising approach recently used in the delivery of chemotherapy drugs and

Table 6. Comparison of the Bax/Bcl-2 ratio in HNO-97 TSCC cells following treatment with different $IC_{50}$ concentrations of Q, QNPs, NVs and DOX after 4 and 24 hours of incubation.

| Time | NVs | | Q | | QNPs | | DOX | | *P* value | $\eta^2$ |
|---|---|---|---|---|---|---|---|---|---|---|
| | Mean | SD | Mean | SD | Mean | SD | Mean | SD | | |
| 4 h | 1.04 $^{D}$ | 0.04 | 4.54 $^{B}$ | 0.11 | 13.92 $^{A}$ | 0.72 | 2.43 $^{C}$ | 0.03 | <0.001* | 0.997 |
| 24 h | 1.00 $^{C}$ | 0.02 | 6.34 $^{B}$ | 0.16 | 31.03 $^{A}$ | 3.36 | 5.13 $^{B}$ | 0.19 | <0.001* | 0.987 |

$^{A,B,C,D}$Different superscripts in the same row indicate statistically significant differences between experimental formulations; DOX, doxorubicin; NVs, PLGA-PEG nanovoids; Q, quercetin; and QNPs, quercetin-loaded PLGA-PEG nanoparticles. *Significant, $P \leq 0.05$; $\eta^2$, Effect size (Partial Eta Squared).

Despite their potency and ease of production, synthetic anticancer drugs are limited by toxicity, adverse side effects, and resistance [32-35]. Phytochemicals derived from dietary sources are increasingly recognized as potential alternatives for cancer treatment [36, 37] . Q, a naturally occurring flavonoid, has attracted attention because of its broad-spectrum pharmacological properties. It may be a potential chemotherapeutic agent and a promising candidate for various types of cancer [10, 38, 39]. However, its potential efficacy is hindered by poor water solubility, low bioavailability, and short biological half-life [40, 41].

To address these limitations, this study used a delivery system based on PLGA-PEG NPs to encapsulate Q and assessed its antitumour activity in the HNO-97 TSCC cell line. This study compared the cytotoxic, apoptotic, and gene expression-modulatory effects of free Q, QNPs, and DOX.

Our results demonstrated that the QNPs exhibited greater antitumour activity than free Q in HNO-97 cells. Crucially, the extremely low cytotoxicity of the NVs supported their use as safe anticancer agent delivery vehicles and confirmed their biocompatibility. Comparable results were observed in other models, where NVs based on PLGA-PEG were nontoxic to cancer and healthy cells [24].

MTT assays revealed a time-dependent increase in the antiproliferative activity of the QNPs. After 4 hours, free Q demonstrated greater cytotoxicity, reducing cell viability to 18.3% at 100 µM, compared with 44.9% for the QNPs. However, by 24 hours, the QNPs significantly outperformed both the Q and the DOX, reducing the cell viability to 2.6%, whereas it was 14.0% for the Q and 44.4% for the DOX. This delayed effect of the QNPs can be attributed to the controlled release characteristics of the PLGA-PEG NPs, which enabled the gradual release of Q into the cellular environment. These results are consistent with those of previous studies on different cancer models that emphasized improved intracellular delivery of Q via PLGA-PEG NPs [42-44]. Moreover, the enhanced cytotoxic activity of the QNPs could be attributed to their small size, which improved their internalization into cancer cells by endocytosis, especially clathrin- and caveolae-independent endocytosis [45, 46]. In addition, PEGylation enhances the permeability and retention effect, which results in better accumulation of drugs in cancer cells [47].

Similarly, Q exhibited $IC_{50}$ values of 58.8 µM and 59.7 µM after 4 and 24 hours of incubation, respectively, which aligned with the findings of Huang et al., who reported an $IC_{50}$ of ~50 µM for free Q after 24 hours in TSCC SAS cells [23]. Previously published studies have reported a wide range of $IC_{50}$ values for Q in OSCC cell lines, typically ranging from 5 µM to 160 µM, depending on the cell type, exposure time, and experimental conditions [36, 48-52]. In our study, the $IC_{50}$ value of Q for HNO-97 TSCC cells was 59.7 ± 1.3 µM at 24 hours, which falls well within the range reported in the literature. Notably, the QNPs had the lowest $IC_{50}$ value (41.4 µM) after 24 hours, confirming their superior long-term cytotoxic efficacy because of the sustained drug release profile of the PLGA-PEG NP formulation. A similar finding has been reported in other cancer models, where Q-loaded PLGA NPs enhance the cytotoxicity and $IC_{50}$ values in a time-dependent manner [39].

Although doxorubicin (DOX) was used as a positive control to benchmark the cytotoxic effects of Q and QNPs, the $IC_{50}$ value observed in our study (~74.7 μM) is notably higher than those typically reported in the literature (0.5–5 μM). This elevated value may reflect an inherent resistance phenotype of the HNO-97 TSCC cell line. Several mechanisms could explain the reduced sensitivity to DOX. Christowitz et al [53] demonstrated that activation of the MAPK/ERK signalling pathway contributes to DOX resistance in murine E0771 breast cancer cells. Similarly, Du et al.[54] reported that microRNA-221 overexpression in SCC4 and SCC9 OSCC cell lines led to the downregulation of tissue inhibitor of metalloproteinase 3 (TIMP3), thereby promoting DOX resistance. Additionally, DOX's poor tissue permeability and limited diffusion capacity, as reported by Primeau et al.[55], may further hinder its intracellular accumulation and therapeutic efficacy. Therefore, while QNPs demonstrated greater cytotoxicity in this specific model, this result should be interpreted with caution. The observed superiority of QNPs over DOX may be influenced by the resistance profile of the HNO-97 cell line, and it is not appropriate to generalize this finding without broader validation.

A prominent apoptotic response was observed in the QNPs-treated cells, with flow cytometry analysis revealing the highest significant induction rate of late apoptosis compared with free Q and DOX (87.6%), particularly after 24 hours. In addition to increasing the cytotoxic effect of Q, this finding also highlighted that the encapsulation of Q in PLGA-PEG NPs greatly amplified its ability to induce apoptosis over time. These results aligned with those of previous studies conducted on other cancer models, which demonstrated that PLGA and PLGA-PEG nanoparticle-mediated delivery of Q increased its bioavailability and intracellular accumulation, thereby promoting more effective apoptotic responses in cancer cells [44, 56].

The expression levels of the Bax, Bcl-2, and PI3K genes were investigated better to understand the underlying mechanism of cancer cell death. After 24 hours, the results revealed that Q notably upregulated Bax gene expression and downregulated Bcl-2, and the QNPs significantly and time-dependently acted as powerful anticancer agents. The highest upregulation activity of the proapoptotic gene Bax and the lowest downregulation activity of the antiapoptotic gene Bcl-2, and the survival-associated gene PI3K were recorded. As a result, the highest Bax/Bcl-2 ratio was recorded in the QNPs-treated cells (31.03), which was greater than that in the cells treated with free Q (6.34) and DOX (5.13). This finding supported the enhanced activation of the intrinsic apoptotic pathway by the QNPs and strongly correlated with the high percentage of late apoptotic cells observed via flow cytometry analysis. This ratio is indicative of robust proapoptotic signalling and has been widely accepted as a hallmark of the anticancer effectiveness of the encapsulation of Q into NPs [57, 58]. Based on the PCR analysis results, it can be inferred that mitochondria may represent key targets of Q. This hypothesis is supported by earlier studies indicating that Q disrupted the mitochondrial membrane potential, thereby inducing mitochondrial dysfunction and contributing to apoptotic cell death [36].

The pronounced suppression of the PI3K gene observed in this study suggested that the QNPs suppressed cancer cell survival by inhibiting the PI3K/AKT pathway, which contributed to QNPs-mediated anticancer activity. These results imply that Q's capacity to modify apoptotic and survival signalling pathways is greatly enhanced by PLGA-PEG encapsulation, outperforming both free Q and DOX. Similar outcomes have been reported in previous studies, where QNPs promoted apoptosis through Bax upregulation and Bcl-2 downregulation, alongside the inhibition of survival signalling via PI3K suppression in various cancer cell lines [56, 59-61].

The results of this study collectively imply that the use of Q PLGA-PEG NPs could be a useful nanotherapeutic approach for the treatment of TSCC. They have the potential to be useful in preclinical and clinical settings in the future because of their capacity to increase cytotoxicity, strongly induce apoptosis, and inhibit important survival pathways, such as the PI3K pathway. While our findings support the potential of QNPs as natural-based nanotherapeutic anticancer agents for the HNO-97 TSCC cell line, this study has several limitations. The use of a single TSCC cell line may restrict the generalizability of our findings across the

broader spectrum of OSCC. HNO-97 cells were selected based on institutional availability and their clinical relevance as a well-characterized TSCC model. However, future studies incorporating multiple TSCC and OSCC cell lines will be essential to validate and expand the applicability of these results.

Additionally, the actual clinical and physiological complexity of the tumor microenvironment is not accurately simulated by an in vitro model, which is based on the application of experimental anticancer drugs loaded into NPs to cultured cancer cells. Further investigations in animal models are needed to assess pharmacokinetics, biodistribution, systemic toxicity, and therapeutic efficacy under physiological conditions. These future studies will be critical to establishing the translational potential of QNPs as a nanotherapeutic strategy for TSCC. Finally, it is essential to note that changes in gene expression, including PI3K, may reflect downstream effects of cell stress or death rather than direct regulatory events. Therefore, further studies involving protein-level validation and mechanistic dissection are needed to confirm the functional significance of these findings.

## Conclusion

Q exhibited dose-dependent anticancer effects on HNO-97 TSCC cells. The results demonstrated that the encapsulation of Q within PLGA-PEG NPs significantly enhanced the therapeutic potential of Q by reducing proliferation, decreasing the $IC_{50}$ values, increasing the late apoptosis rate, modulating the expression of apoptosis-related genes, and preventing HNO-97 cell survival in a time-dependent manner, outperforming both free Q and DOX.

## Abbreviations

EE: Entrapment efficiency; NVs: Nanovoids; OSCC, Oral Squamous Cell Carcinoma; SCC, Squamous Cell Carcinoma

Ethics approval. This study was approved by the Research Ethical Committee at the Faculty of Dentistry, Cairo University (number: 6722).

Availability of data: Original data is included in the article. Any further inquiries can be directed to the corresponding authors.

Author Contributions: Conceptualization, H.H.A., and A.A.A.; Methodology, A.A.A. and H.H.A.; Investigation, H.H.A., and A.A.A.; Formal analysis, H.H.A., and A.A.A.; Project administration, H.H.A.; Resources, H.H.A.; Supervision, N.R.A. and A.A.A.; Validation: A.A.A.; Writing—original draft, H.H.A.; Data curation, A.A.A.; Writing, review and editing, N.R.A., A.A.A. and O.A.B. All authors have read and agreed to the published version of the manuscript.

Funding: This research received no external funding.

Acknowledgments: N/A

Conflicts of Interest: The authors declare no conflict of interest.

Quote this article as Algadi, Hana'a Hezam, Ahmed A. Abd-Rabou, Omnia A. Badawi, Nada Noureldin, and Nermine Raouf Amin. 2025. "Therapeutic Efficacy of Quercetin versus Its Encapsulated Nanoparticle on Tongue Squamous Cell Carcinoma Cell Line. Precis. Nanomed. 2025, 8(3):1570-1586 https://doi.org/10.33218/001c.143324.



## References

[1] B. P. George, R. Chandran, and H. Abrahamse, "Role of Phytochemicals in Cancer Chemoprevention: Insights," (in eng), *Antioxidants (Basel),* vol. 10, no. 9, Sep 14 2021, doi: 10.3390/antiox10091455.

[2] M. Zhang, J. Liang, Y. Yang, H. Liang, H. Jia, and D. Li, "Current Trends of Targeted Drug Delivery for Oral Cancer Therapy," (in English), *Frontiers in Bioengineering and Biotechnology,* Review vol. Volume 8 - 2020, 2020-December-08 2020, doi: 10.3389/fbioe.2020.618931.

[3] P. Pradeep Prabhu *et al.*, "Harnessing the nutriceutics in early-stage breast cancer: mechanisms, combinational therapy, and drug delivery," *Journal of Nanobiotechnology,* vol. 22, no. 1, p. 574, 2024/09/18 2024, doi: 10.1186/s12951-024-02815-8.
[4] M. Chehelgerdi *et al.*, "Progressing nanotechnology to improve targeted cancer treatment: overcoming hurdles in its clinical implementation," (in eng), *Mol Cancer,* vol. 22, no. 1, p. 169, Oct 9 2023, doi: 10.1186/s12943-023-01865-0.
[5] M. Z. Saavedra-Leos, E. Jordan-Alejandre, C. López-Camarillo, A. Pozos-Guillen, C. Leyva-Porras, and M. B. Silva-Cázares, "Nanomaterial Complexes Enriched With Natural Compounds Used in Cancer Therapies: A Perspective for Clinical Application," (in English), *Frontiers in Oncology,* Review vol. 11, 2021-April-01 2021, doi: 10.3389/fonc.2021.664380.
[6] L. Gibellini *et al.*, "Quercetin and cancer chemoprevention," (in eng), *Evid Based Complement Alternat Med,* vol. 2011, p. 591356, 2011, doi: 10.1093/ecam/neq053.
[7] S. Srivastava *et al.*, "Quercetin, a Natural Flavonoid Interacts with DNA, Arrests Cell Cycle and Causes Tumor Regression by Activating Mitochondrial Pathway of Apoptosis," (in eng), *Sci Rep,* vol. 6, p. 24049, Apr 12 2016, doi: 10.1038/srep24049.
[8] M. Hashemzaei *et al.*, "Anticancer and apoptosis-inducing effects of quercetin in vitro and in vivo," (in eng), *Oncol Rep,* vol. 38, no. 2, pp. 819-828, Aug 2017, doi: 10.3892/or.2017.5766.
[9] J. Zhou *et al.*, "Investigation of the anticancer effect of quercetin on HepG2 cells in vivo," (in eng), *PLoS One,* vol. 12, no. 3, p. e0172838, 2017, doi: 10.1371/journal.pone.0172838.
[10] N. Lotfi *et al.*, "The potential anticancer effects of quercetin on blood, prostate and lung cancers: An update," (in eng), *Front Immunol,* vol. 14, p. 1077531, 2023, doi: 10.3389/fimmu.2023.1077531.
[11] J. Lu *et al.*, "Quercetin Inhibits the Migration and Invasion of HCCLM3 Cells by Suppressing the Expression of p-Akt1, Matrix Metalloproteinase (MMP) MMP-2, and MMP-9," (in eng), *Medical science monitor : international medical journal of experimental and clinical research,* vol. 24, pp. 2583-2589, Apr 27 2018, doi: 10.12659/msm.906172.
[12] C. Y. Chan, C. H. Lien, M. F. Lee, and C. Y. Huang, "Quercetin suppresses cellular migration and invasion in human head and neck squamous cell carcinoma (HNSCC)," (in eng), *BioMedicine,* vol. 6, no. 3, p. 15, Jun 2016, doi: 10.7603/s40681-016-0015-3.
[13] A. D. Marrero, A. R. Quesada, B. Martínez-Poveda, and M. Medina, "Antiangiogenic Phytochemicals Constituent of Diet as Promising Candidates for Chemoprevention of Cancer," (in eng), *Antioxidants (Basel),* vol. 11, no. 2, Jan 31 2022, doi: 10.3390/antiox11020302.
[14] M. Vinayak and A. K. Maurya, "Quercetin Loaded Nanoparticles in Targeting Cancer: Recent Development," (in eng), *Anticancer Agents Med Chem,* vol. 19, no. 13, pp. 1560-1576, 2019, doi: 10.2174/1871520619666190705150214.
[15] Y. Zhu, L. M. Wen, R. Li, W. Dong, S. Y. Jia, and M. C. Qi, "Recent advances of nano-drug delivery system in oral squamous cell carcinoma treatment," (in eng), *Eur Rev Med Pharmacol Sci,* vol. 23, no. 21, pp. 9445-9453, Nov 2019, doi: 10.26355/eurrev_201911_19438.
[16] Y. Li, T. Thambi, and D. S. Lee, "Co-Delivery of Drugs and Genes Using Polymeric Nanoparticles for Synergistic Cancer Therapeutic Effects," *Advanced Healthcare Materials,* vol. 7, no. 1, p. 1700886, 2018, doi: https://doi.org/10.1002/adhm.201700886.
[17] S. Sur, A. Rathore, V. Dave, K. R. Reddy, R. S. Chouhan, and V. Sadhu, "Recent developments in functionalized polymer nanoparticles for efficient drug delivery system," *Nano-Structures & Nano-Objects,* vol. 20, p. 100397, 2019/10/01/ 2019, doi: https://doi.org/10.1016/j.nanoso.2019.100397.
[18] R. Gref *et al.*, "'Stealth' corona-core nanoparticles surface modified by polyethylene glycol (PEG): influences of the corona (PEG chain length and surface density) and of the core composition on phagocytic uptake and plasma protein adsorption," *Colloids Surf B Biointerfaces,* vol. 18, no. 3-4, pp. 301-313, Oct 1 2000, doi: 10.1016/s0927-7765(99)00156-3.
[19] S.-F. Chen, S. Nien, C.-H. Wu, C.-L. Liu, Y.-C. Chang, and Y.-S. Lin, "Reappraisal of the anticancer efficacy of quercetin in oral cancer cells," (in eng), *J Chin Med Assoc,* vol. 76, no. 3, pp. 146-152, 2013/03// 2013, doi: 10.1016/j.jcma.2012.11.008.
[20] L. Chen, J. S. Xia, J. H. Wu, Y. G. Chen, and C. J. Qiu, "Quercetin suppresses cell survival and invasion in oral squamous cell carcinoma via the miR-1254/CD36 cascade in vitro," (in eng), *Hum Exp Toxicol,* vol. 40, no. 9, pp. 1413-1421, Sep 2021, doi: 10.1177/0960327121991912.
[21] W. Zhang, G. Yin, J. Dai, Y. Sun, R. Hoffman, and Z. Yang, "Chemoprevention by Quercetin of Oral Squamous Cell Carcinoma by Suppression of the NF-κB Signaling Pathway in DMBA-treated

Hamsters," *Anticancer Research,* vol. 37, pp. 4041-4050, 08/01 2017, doi: 10.21873/anticanres.11789.
[22] C. Zhang, Y. Hao, Y. Sun, and P. Liu, "Quercetin suppresses the tumorigenesis of oral squamous cell carcinoma by regulating microRNA-22/WNT1/β-catenin axis," (in eng), *J Pharmacol Sci,* vol. 140, no. 2, pp. 128-136, Jun 2019, doi: 10.1016/j.jphs.2019.03.005.
[23] C. F. Huang *et al.*, "Quercetin induces tongue squamous cell carcinoma cell apoptosis via the JNK activation-regulated ERK/GSK-3α/β-mediated mitochondria-dependent apoptotic signaling pathway," (in eng), *Oncol Lett,* vol. 23, no. 3, p. 78, Mar 2022, doi: 10.3892/ol.2022.13198.
[24] A. A. Abd-Rabou and H. H. Ahmed, "CS-PEG decorated PLGA nano-prototype for delivery of bioactive compounds: A novel approach for induction of apoptosis in HepG2 cell line," *Advances in Medical Sciences,* vol. 62, no. 2, pp. 357-367, 2017/09/01/ 2017, doi: https://doi.org/10.1016/j.advms.2017.01.003.
[25] M. F. El-Ssayad, A. A. Abd-Rabou, and H. S. El-Sayed, "Utilization of lactobacilli extracts as antibacterial agent and to induce colorectal cancer cells apoptosis: Application in white soft cheese," *Food Bioscience,* vol. 56, p. 103252, 2023/12/01/ 2023, doi: https://doi.org/10.1016/j.fbio.2023.103252.
[26] K. J. Livak and T. D. Schmittgen, "Analysis of Relative Gene Expression Data Using Real-Time Quantitative PCR and the 2−ΔΔCT Method," *Methods,* vol. 25, no. 4, pp. 402-408, 2001/12/01/ 2001, doi: https://doi.org/10.1006/meth.2001.1262.
[27] A. F. Hashim, A. A. Abd-Rabou, and H. S. El-Sayed, "Functional nanoemulsion and nanocomposite microparticles as an anticolorectal cancer and antimicrobial agent: applied in yogurt," *Biomass Conversion and Biorefinery,* vol. 14, no. 12, pp. 13233-13249, 2024/06/01 2024, doi: 10.1007/s13399-022-03313-3.
[28] A. A. Abd-Rabou, A. M. Abdelaziz, O. G. Shaker, and G. Ayeldeen, "Hyaluronated nanoparticles deliver raloxifene to CD44-expressed colon cancer cells and regulate lncRNAs/miRNAs epigenetic cascade," *Cancer Nanotechnology,* vol. 14, no. 1, p. 32, 2023/04/07 2023, doi: 10.1186/s12645-023-00183-w.
[29] A. A. Mostafa, M. M. H. El-Sayed, A. N. Emam, A. A. Abd-Rabou, R. M. Dawood, and H. Oudadesse, "Bioactive glass doped with noble metal nanoparticles for bone regeneration: in vitro kinetics and proliferative impact on human bone cell line," *RSC Advances,* 10.1039/D1RA03876A vol. 11, no. 41, pp. 25628-25638, 2021, doi: 10.1039/D1RA03876A.
[30] Y. Chen *et al.*, "Polymer-based nanoparticles for chemo/gene-therapy: Evaluation its therapeutic efficacy and toxicity against colorectal carcinoma," *Biomedicine & Pharmacotherapy,* vol. 118, p. 109257, 2019/10/01/ 2019, doi: https://doi.org/10.1016/j.biopha.2019.109257.
[31] L. Faramarzi, M. Dadashpour, H. Sadeghzadeh, M. Mahdavi, and N. Zarghami, "Enhanced antiproliferative and proapoptotic effects of metformin encapsulated PLGA-PEG nanoparticles on SKOV3 human ovarian carcinoma cells," *Artificial cells, nanomedicine, and biotechnology,* vol. 47, no. 1, pp. 737-746, 2019.
[32] E. M. Emara, W. A. El-Sayed, A. S. A. Khalaf-Allah, F. M. Alminderej, Y. K. Abdel-Monem, and A. A. Abd-Rabou, "Spectral studies, thermal investigations, and anticancer activity of some divalent metal complexes derived from 2-(4-bromophenylamino)acetohydrazide ligand," *Applied Organometallic Chemistry,* vol. 36, no. 5, p. e6657, 2022, doi: https://doi.org/10.1002/aoc.6657.
[33] E. Mansour, A. A. Abd-Rabou, S. S. Zaghlool, A. M. Sayed, I. F. Nassar, and S. I. Elewa, "Novel indoline analogues reverse resistant breast cancer via p-glycoprotein inhibition and apoptotic genes modulation," *Journal of Molecular Structure,* vol. 1331, p. 141471, June 01, 2025 2025, doi: 10.1016/j.molstruc.2025.141471.
[34] W. I. El-Sofany, D. A. A. Osman, A. M. Mahran, A. A. Abd-Rabou, and N. Tawfek, "Microwave assists synthesis of spirothiazolidine derivatives to induce cervical cancer cell death-mediated apoptosis in vitro," *Journal of Molecular Structure,* vol. 1294, p. 136424, 2023/12/15/ 2023, doi: https://doi.org/10.1016/j.molstruc.2023.136424.
[35] H. K. A. El-Mawgoud, A. A. Abd-Rabou, M. A. El-Atawy, H. A. Ahmed, and E. Mansour, "Synthesis, DFT analysis, and molecular docking of pyrazole derivatives as targeted inhibitors of PI3K/AKT and JAK/STAT pathways in lung cancer cells," *Journal of Molecular Structure,* vol. 1334, p. 141875, 2025/07/05/ 2025, doi: https://doi.org/10.1016/j.molstruc.2025.141875.

[36] Y. S. Ma *et al.*, "Quercetin induced apoptosis of human oral cancer SAS cells through mitochondria and endoplasmic reticulum mediated signaling pathways," *Oncol Lett,* vol. 15, no. 6, pp. 9663-9672, 2018/06/01 2018, doi: https://doi.org/10.3892/ol.2018.8584.

[37] L. Chen, J.-s. Xia, J.-H. Wu, Y.-G. Chen, and C.-J. Qiu, "Quercetin suppresses cell survival and invasion in oral squamous cell carcinoma via the miR-1254/CD36 cascade in vitro," *Human & Experimental Toxicology,* vol. 40, pp. 1413 - 1421, 2021.

[38] F. Sheikhnia *et al.*, "Exploring the therapeutic potential of quercetin in cancer treatment: Targeting long non-coding RNAs," *Pathology - Research and Practice,* vol. 260, p. 155374, 2024/08/01/ 2024, doi: https://doi.org/10.1016/j.prp.2024.155374.

[39] H. Dong *et al.*, "Using network pharmacological analysis and molecular docking to investigate the mechanism of action of quercetin's suppression of oral cancer," (in eng), *J Cancer Res Clin Oncol,* vol. 149, no. 16, pp. 15055-15067, Nov 2023, doi: 10.1007/s00432-023-05290-0.

[40] X. Cai, Z. Fang, J. Dou, A. Yu, and G. Zhai, "Bioavailability of Quercetin: Problems and Promises," *Current Medicinal Chemistry,* vol. 20, no. 20, pp. 2572-2582, 2013, doi: http://dx.doi.org/10.2174/09298673113209990120.

[41] Y. Guo and R. S. Bruno, "Endogenous and exogenous mediators of quercetin bioavailability," *The Journal of Nutritional Biochemistry,* vol. 26, no. 3, pp. 201-210, 2015/03/01/ 2015, doi: https://doi.org/10.1016/j.jnutbio.2014.10.008.

[42] M. Ersoz, A. Erdemir, S. Derman, T. Arasoglu, and B. Mansuroglu, "Quercetin-loaded nanoparticles enhance cytotoxicity and antioxidant activity on C6 glioma cells," *Pharmaceutical Development and Technology,* vol. 25, no. 6, pp. 757-766, 2020/07/02 2020, doi: 10.1080/10837450.2020.1740933.

[43] Q. Lu *et al.*, "Co-delivery of Paclitaxel/Atovaquone/Quercetin to regulate energy metabolism to reverse multidrug resistance in ovarian cancer by PLGA-PEG nanoparticles," *International Journal of Pharmaceutics,* vol. 655, p. 124028, 2024/04/25/ 2024, doi: https://doi.org/10.1016/j.ijpharm.2024.124028.

[44] A. A. Shitole *et al.*, "LHRH-conjugated, PEGylated, poly-lactide-co-glycolide nanocapsules for targeted delivery of combinational chemotherapeutic drugs Docetaxel and Quercetin for prostate cancer," *Materials Science and Engineering: C,* vol. 114, p. 111035, 2020/09/01/ 2020, doi: https://doi.org/10.1016/j.msec.2020.111035.

[45] D. Manzanares and V. Ceña, "Endocytosis: The Nanoparticle and Submicron Nanocompounds Gateway into the Cell," (in eng), *Pharmaceutics,* vol. 12, no. 4, Apr 17 2020, doi: 10.3390/pharmaceutics12040371.

[46] A. Platel, R. Carpentier, E. Becart, G. Mordacq, D. Betbeder, and F. Nesslany, "Influence of the surface charge of PLGA nanoparticles on their in vitro genotoxicity, cytotoxicity, ROS production and endocytosis," *Journal of Applied Toxicology,* vol. 36, no. 3, pp. 434-444, 2016, doi: https://doi.org/10.1002/jat.3247.

[47] E. Locatelli and M. Comes Franchini, "Biodegradable PLGA-b-PEG polymeric nanoparticles: synthesis, properties, and nanomedical applications as drug delivery system," *Journal of Nanoparticle Research,* vol. 14, no. 12, p. 1316, 2012/11/25 2012, doi: 10.1007/s11051-012-1316-4.

[48] S. R. Kim, E. Y. Lee, D. J. Kim, H. J. Kim, and H. R. Park, "Quercetin Inhibits Cell Survival and Metastatic Ability via the EMT-Mediated Pathway in Oral Squamous Cell Carcinoma," *Molecules,* vol. 25, no. 3, p. 757, 2020. [Online]. Available: https://www.mdpi.com/1420-3049/25/3/757.

[49] C.-Y. Chan, S.-C. Hong, C.-M. Chang, Y.-H. Chen, P.-C. Liao, and C.-Y. Huang, "Oral Squamous Cell Carcinoma Cells with Acquired Resistance to Erlotinib Are Sensitive to Anticancer Effect of Quercetin via Pyruvate Kinase M2 (PKM2)," *Cells,* vol. 12, no. 1, p. 179, 2023. [Online]. Available: https://www.mdpi.com/2073-4409/12/1/179.

[50] J. Zhao *et al.*, "Quercetin inhibits cell viability, migration and invasion by regulating miR-16/HOXA10 axis in oral cancer," *European Journal of Pharmacology,* vol. 847, pp. 11-18, 2019/03/15/ 2019, doi: https://doi.org/10.1016/j.ejphar.2019.01.006.

[51] C. Zhang, Y. Hao, Y. Sun, and P. Liu, "Quercetin suppresses the tumorigenesis of oral squamous cell carcinoma by regulating microRNA-22/WNT1/β-catenin axis," *Journal of Pharmacological Sciences,* vol. 140, no. 2, pp. 128-136, 2019/06/01/ 2019, doi: https://doi.org/10.1016/j.jphs.2019.03.005.

[52] C.-Y. Huang, C.-Y. Chan, I. T. Chou, C.-H. Lien, H.-C. Hung, and M.-F. Lee, "Quercetin induces growth arrest through activation of FOXO1 transcription factor in EGFR-overexpressing oral cancer

cells," *The Journal of Nutritional Biochemistry,* vol. 24, no. 9, pp. 1596-1603, 2013/09/01/ 2013, doi: https://doi.org/10.1016/j.jnutbio.2013.01.010.

[53] C. Christowitz, T. Davis, A. Isaacs, G. van Niekerk, S. Hattingh, and A.-M. Engelbrecht, "Mechanisms of doxorubicin-induced drug resistance and drug resistant tumour growth in a murine breast tumour model," *BMC Cancer,* vol. 19, no. 1, p. 757, 2019/08/01 2019, doi: 10.1186/s12885-019-5939-z.

[54] L. Du, S. Ma, X. Wen, J. Chai, and D. Zhou, "Oral squamous cell carcinoma cells are resistant to doxorubicin through upregulation of miR-221," *Mol Med Rep,* vol. 16, no. 3, pp. 2659-2667, 2017/09/01 2017, doi: 10.3892/mmr.2017.6915.

[55] A. J. Primeau, A. Rendon, D. Hedley, L. Lilge, and I. F. Tannock, "The distribution of the anticancer drug Doxorubicin in relation to blood vessels in solid tumors," (in eng), *Clin Cancer Res,* vol. 11, no. 24 Pt 1, pp. 8782-8, Dec 15 2005, doi: 10.1158/1078-0432.Ccr-05-1664.

[56] N. Yadav, A. K. Tripathi, A. Parveen, S. Parveen, and M. Banerjee, "PLGA-Quercetin Nano-Formulation Inhibits Cancer Progression via Mitochondrial Dependent Caspase-3,7 and Independent FoxO1 Activation with Concomitant PI3K/AKT Suppression," *Pharmaceutics,* vol. 14, no. 7, p. 1326, 2022. [Online]. Available: https://www.mdpi.com/1999-4923/14/7/1326.

[57] F. Niazvand, M. Orazizadeh, L. Khorsandi, M. Abbaspour, E. Mansouri, and A. Khodadadi, "Effects of Quercetin-Loaded Nanoparticles on MCF-7 Human Breast Cancer Cells," *Medicina,* vol. 55, no. 4, p. 114, 2019. [Online]. Available: https://www.mdpi.com/1648-9144/55/4/114.

[58] R. Afarin, F. Ahmadpour, M. Hatami, S. Monjezi, and S. Igder, "Combination of Etoposide and quercetin-loaded solid lipid nanoparticles Potentiates apoptotic effects on MDA-MB-231 breast cancer cells," *Heliyon,* vol. 10, no. 11, 2024, doi: 10.1016/j.heliyon.2024.e31925.

[59] J. Duo, G.-G. Ying, G.-W. Wang, and L. Zhang, "Quercetin inhibits human breast cancer cell proliferation and induces apoptosis via Bcl-2 and Bax regulation," *Mol Med Rep,* vol. 5, no. 6, pp. 1453-1456, 2012/06/01 2012, doi: 10.3892/mmr.2012.845.

[60] A. M. W. Hasan *et al.*, "Quercetin promises anticancer activity through PI3K-AKT-mTOR pathway: A literature review," *Pharmacological Research - Natural Products,* vol. 7, p. 100206, 2025/06/01/ 2025, doi: https://doi.org/10.1016/j.prenap.2025.100206.

[61] M. Hatami, M. Kouchak, A. Kheirollah, L. Khorsandi, and M. Rashidi, "Quercetin-loaded solid lipid nanoparticles exhibit antitumor activity and suppress the proliferation of triple-negative MDA-MB 231 breast cancer cells: implications for invasive breast cancer treatment," (in eng), *Mol Biol Rep,* vol. 50, no. 11, pp. 9417-9430, Nov 2023, doi: 10.1007/s11033-023-08848-w.